MOLECULAR IMAGING AND BIOLOGY

Published Online: 23 September 2010

Mol Imaging Biol (2011) 13:599–612
DOI: 10.1007/s11307-010-0421-y

REVIEW ARTICLE

Preclinical Lymphatic Imaging

Fan Zhang,[1,2] Gang Niu,[1,3] Guangming Lu,[2] Xiaoyuan Chen[1]

[1]*Laboratory of Molecular Imaging and Nanomedicine (LOMIN), National Institute of Biomedical Imaging and Bioengineering (NIBIB), National Institutes of Health (NIH), 31 Center Drive, Suite 1C14, Bethesda, MD 20892, USA*
[2]*Department of Radiology, Nanjing Jinling Hospital, Clinical School of Medical College of Nanjing University, Nanjing 210002, China*
[3]*Imaging Sciences Training Program, Radiology and Imaging Sciences, Clinical Center and National Institute Biomedical Imaging and Bioengineering, 9 Memorial Drive, 9/1W111, NIH, Bethesda, MD 20892, USA*

Abstract

Noninvasive *in vivo* imaging of lymphatic vessels and lymphatic nodes is expected to fulfill the purpose of analyzing lymphatic vessels and their function, understanding molecular mechanisms of lymphangiogenesis and lymphatic spread of tumors, and utilizing lymphatic molecular markers as a prognostic or diagnostic indicator. In this review, we provide a comprehensive summary of *in vivo* imaging modalities for detecting lymphatic vessels, lymphatic drainage, and lymphatic nodes, which include conventional lymphatic imaging techniques such as dyes and radionuclide scintigraphy as well as novel techniques for lymphatic imaging such as optical imaging, computed tomography, magnetic resonance imaging, ultrasound, positron emission tomography using lymphatic biomarkers, photoacoustic imaging, and combinations of multiple modalities. The field of lymphatic imaging is ever evolving, and technological advances, combined with the development of new contrast agents, continue to improve the research of lymphatic vascular system in health and disease states as well as to improve the accuracy of diagnosis in the relevant diseases.

Key words: Lymphatic imaging, Lymphangiography, Contrast agent, Molecular imaging

Introduction

The lymphatic system is a complex network of lymphatic vessels, lymph nodes, and other lymphatic organs, which are essential for the maintenance of fluid homeostasis and immunocompetence. Lymphatic vessels are found in nearly every organ and blood vessel-containing interstitial tissue and serve as a drainage system for excess fluid and large molecules or cells that cannot easily find their way back into venules [1, 2]. Although lymphatic vessels were first described back in the seventeenth century, the first growth factors and molecular markers specific for these vessels were not discovered until a decade ago [3, 4]. Much progress has been made in recent years including the discovery of key molecular pathways regulating lymphangiogenesis, the identification of lymphangiogenesis markers, the isolation of lymphatic endothelial cells, and the development of genetically modified animal models to study lymphangiogenesis [3–12].

The lymphatic vessels contribute to a wide range of human pathologies, such as cancer metastases [3, 13, 14], inflammation [15–17], diabetes [18], and obesity [19]. Especially in cancer metastasis, the lymphatic system transports fluid and cells from the periphery to the circulation. This system is increasingly appreciated as a conduit for the metastasis of a variety of human cancers such as breast, melanoma, and head and neck cancers [3]. Thus, investigation of the lymphatic contribution to metastasis may lead to diagnostic or therapeutic strategies to identify or prevent

Correspondence to: Gang Niu; *e-mail:* niug@mail.nih.gov, Xiaoyuan Chen; *e-mail:* shawn.chen@nih.gov

tumor dissemination. At present, some new *in vivo* models rapidly provide an abundance of information on the mechanisms underlying lymphatic development and the progression of diseases associated with lymphatic dysfunction [9]. Yet, compared with *in vivo* hemovascular imaging, lymphatics imaging has been paid much less attention [20]. Although technically challenging, the ability to image lymph flow, lymph nodes, lymphatic function, and markers of lymphangiogenesis could have a profound impact on our understanding of these diseases.

Imaging of the hemovascular system often requires intravenous administration of contrast agents, while the routes of introducing contrast agents into the lymphatics are through interstitial (intradermal or subcutaneous) administration, direct administration into lymphatic vessel, or intravenous injection. Small nanoparticles can pool into the lymph nodes via blood circulation, but can also diffuse into lymphatic vessels via the gap junctions between the endothelial cells under a hydrostatic pressure gradient. Particles between 10 and 100 nm in diameter can extravasate into the interstitial space, where they are phagocytosed by macrophages and are then transported to lymph nodes. Particles larger than 100 nm typically remain trapped in the interstitium [20, 21]. In the following sections, we will review various imaging modalities and contrast agents used for lymphatic imaging with focus on preclinical studies that have translational potential.

Conventional Lymphatic Imaging

Conventional lymphatic imaging using dyes and radionuclide scintigraphy has a long history. These methods delineate not only lymphatic vessels and drainage but also sentinel lymph nodes (SLN). Blue dye staining has been the principal method of determining blood volume in humans and animals for almost a century. The commonly used dyes are isosulfan blue, patent blue V, Evans blue (EB), or fluorescent dyes (see "Fluorescence Optical Imaging" section), which provide a visual signal of the draining lymphatic vessels and lymph nodes [22]. Since these dyes color living tissues or cells, they are also called vital dyes [23]. Typically, dye molecules are injected intradermally or subcutaneously into the interstitial tissue of animals or human beings, to obtain indirect micro-lymphangiographies of superficial lymphatic vessels. After injection of blue dyes, cutaneous lymphatic vessels and lymphatic drainage from the skin can be macroscopically visualized [19, 22, 24]. Kajiya *et al.* [25] observed prominent enlargement, functionally impaired and hyperpermeable lymphatic vessels of the ultraviolet B-induced cutaneous damage, as well as systemic blockade of VEGF-A inhibited enlargement of lymphatics by injection of Evans blue dye into the rim of mouse ears. Harvey *et al.* [19] showed multiple hypoplastic and tortuous Evans blue dye-positive lymphatic vessels in the thoracic cavity in $Prox1^{+/-}$ mice. This phenomenon may reflect functional inactivation of a single allele of the homeobox gene Prox1 led to adult-onset obesity due to abnormal lymph leakage from mis-patterned and ruptured lymphatic vessels.

Lymphoscintigraphy is a special type of radionuclide imaging which requires injection of gamma-emitting radionuclides labeled macromolecules or larger colloidal particles into a local region of tissue in order to evaluate lymph drainage function by measurement of the removal rate [26]. Lymphoscintigraphy is the most widely used method for lymphedema quantification. Pereira *et al.* [27] provided an easy and rapid lymphatic drainage examination of mammary glands by intramammary administration of ^{99m}Tc-dextran to female mongrel dogs. Anthony *et al.* [28] used ^{99m}Tc-sulfur colloid to study lymphatic regeneration in rat unilateral hind limb autotransplantation models. By gathering quantitative data, they found rapid regeneration of the subcutaneous lymphatics following replantation, which can handle the lymphatic drainage of the limb adequately. This result may explain why there is no clinical lymphedema in human limb and other tissue replants.

SLN is the hypothetical first lymph node or group of nodes reached by metastasizing cancer cells from a primary tumor. Thus, lymph node imaging can be applied to evaluate the metastatic status of a tumor. The basis for SLN imaging is that the contrast agent injected near the primary tumor will be taken up by the adjacent lymphatic system and transported to the SLN. Currently, blue dye and radionuclide-labeled sulfur colloid are the most common imaging agents for SLN imaging. Alex and Krag [29] reported the first gamma-probe localization of SLNs utilizing ^{99m}Tc-sulfur colloid in an animal model. Their study demonstrated that gamma-probe-guided localization could be used to identify and then surgically remove the first draining lymph nodes in 16 inguinal lymphatic basins of eight cats, and this method was found to be comparable to an invasive method using a blue dye. Currently, lymphoscintigraphy has been employed widely in the detection of SLNs. For example, in patients with breast cancer, preoperative lymphoscintigraphy identified SLNs as hot spots 87% of the time, with 20% of the cases showing draining nodes to other basins in addition to or independent of the axilla [30]. Recently, a dual mapping procedure using isotope and dye injections was performed in 60 patients with clinically node-negative breast cancer. SLNs were identified in 59 of 60 patients (98.3%), with a node-positive rate of 41.7% and a false-negative rate of 1.7% [31].

The characteristics and the properties of the agents employed are the major factors governing the efficiency of lymphoscintigraphy. Although ^{99m}Tc-sulfur colloid has higher specificity and lower background radioactivity for lymphatics as compared with ^{99m}Tc-dextran, it has lower solubility in the lymph and requires longer time to obtain satisfactory lymphatic images. Pereira *et al.* [27] injected 18.5 MBq ^{99m}Tc-dextran into the mammary parenchyma around the mammary papilla in adult female mongrel dogs, and their result showed that ^{99m}Tc-dextran mammary

lymphoscintigraphy provided easy and rapid lymphatic drainage examination of mammary glands. In addition to diagnostic imaging, a number of studies have investigated the biodistribution of drug delivery nanoparticles and drug transport to lymph nodes through ^{99m}Tc labeling in order to provide evidence for delivering intralymphatic therapy in the future [32].

Cyclosporine A (CyA) is an important immunosuppressive agent used to prevent allograft rejection in organ and tissue transplantation. Because of its low solubility, bioavailability, and harmful reversible side effects, the clinical treatment is restricted to oral administration. Lymphatic transport seems to be an alternative to improve the therapeutic efficacy of CyA and to exclude its side effects [33, 34]. Kim *et al.* [35] used CyA-loaded ^{99m}Tc-labeled dextran acetate (DxA) and investigated the biodistribution of particles by lymphatic delivery in rats in order to evaluate lymphatic transport effect of CyA. Results indicated that the CyA-loaded ^{99m}Tc-DxA can be well distributed through the lymph nodes. Solid lipid nanoparticles have been proposed as carriers for anti-cancer drugs [36]. Videira *et al.* [37] investigated the biodistribution of ^{99m}Tc-labeled solid lipid nanoparticles by inhalation for pulmonary delivery to the lymphatic drainage in lung cancer. The data showed significant uptake of the radiolabeled nanoparticles into the lymphatics and high rate of distribution in lymph nodes after inhalation.

Because of their quantitative sensitivity, inherent biological safety, and relative ease of use, it is agreed that vital dyes and lymphoscintigraphy hold enormous potential for preclinical and clinical applications. However, these methods have a number of drawbacks. For instance, SLNs need to be dissected to observe blue dye staining, and lymphoscintigraphy has radiation exposure and relatively low resolution. Furthermore, SLN imaging is not applicable to all tumors as not all tumors drain to a single node, hence this technique is not universally applicable. Some novel techniques such as computed tomography (CT), positron emission tomography (PET), ultrasound (US), magnetic resonance imaging (MRI), photoacoustic imaging, and multimodality imaging hold promise in overcoming these drawbacks.

Fluorescence Optical Imaging

Relatively high resolution, no radiation exposure, and ability to image at molecular level have made optical imaging an advancing branch of medical imaging [1]. Optical imaging of the lymphatic system allows for mapping of lymphatic drainage, localization of SLNs, and visualization of multiple nodes [38]. For example, indocyanine green (ICG) is an unconjugated free emissive fluorophore which can be excited at 780 nm with a significant Stoke's shift, enabling fluorescence measurement at 830 nm and greater. ICG is the earliest near-infrared (NIR) dye utilized for the noninvasive detection of tumors in both animals and patients, and has been approved in humans for assessing cardiac and hepatic function as well as lymphatic flow and SLN imaging [39–41]. Kwon *et al.* [42] evaluated propulsive lymph function using ICG in a rodent model. By fixing regions of interest (ROIs) in fluorescent lymph channels and calculating the fluorescence intensity within each ROI, they computed that lymph flow velocity ranged from 0.28 to 1.35 mm/s. Sharma *et al*. [43] also studied the dynamic lymph flow using ICG in a swine model. Following intradermal administration of 3–6 nmol of ICG, lymph flow immediately progressed from the lymphatic plexus, and the lymph vessels and nodes were stained. Lymph flow propelling frequencies were found to be between 0.5 and 3.3 pulses/min and velocities between 0.23 and 0.75 cm/s. ICG has been successfully used to guide SLN biopsy in breast cancer and melanoma by using NIR camera [44–46]. Hirche *et al.* [44] compared SLN detection by ICG optical imaging and by ^{99m}Tc-sulfur radiocolloid scintigraphy in combination with blue dye. Although the sensitivity and specificity of ICG for SLN detection is comparable to conventional methods, the main advantage of this technique is that it allows transcutaneous visualization of intraoperative lymph node detection without radioisotope.

Other NIR organic fluorophores such as Alexa 705, IRDye780, Cy7, and Cy5.5 can also be used to detect lymphatic drainage. These organic fluorophores can also be conjugated with bioactive molecules such as antibodies, proteins, and peptides to effectively enter and remain in the lymphatic system [47]. Hama *et al*. [48] used Cy5.5 and Cy7 conjugated IgG to map the drainage patterns of lymphatic basins and to locate SLNs. In their study, Cy5.5-IgG and Cy7-IgG were injected interstitially into the mammary fat pad, extremity, and ear in a mouse model. One minute after injection, the SLNs of mice were visualized with a depth penetration of approximately 5 mm. The mapping demonstrated that axillary nodes received input of lymph flow from the breast and upper extremity, and cervical nodes received input from the ear and upper extremity.

Most of the organic NIR fluorophores often lack the ideal properties for generating strong fluorescent signals through deep tissue sections. The design of high-emission dipole strength fluorophores is thus necessary for both animal research and clinical imaging applications [47]. The recent advance of nanotechnology has led to the development of quantum dots (Qdots) for use in imaging, detection, and targeting [49–51]. Qdot are nano-sized semiconductor crystals ranging between 5 and 20 nm. The size and shape of Qdots can be fine-tuned to control the emission wavelengths of the Qdots, including ones that emit light in the NIR range [50]. Furthermore, their extreme brightness provides more depth penetration than organic fluorophores. Harrell *et al*. [52] used non-targeted Qdots to demonstrate that increased lymph flow precedes tumor metastasis in a melanoma xenograft model. In their studies, Qtracker 705 particles were injected to the dorsal toe of each hindfoot, and a real-time imaging assay found that tumors can affect lymph flow through the draining lymphatic system. Mean-

while, by measuring the fluorescent signal in an ROI over each popliteal LN, it was found that lymph flow is specifically increased through tumor-draining LNs. Ballou *et al.* [53] also demonstrated that passage from the tumor through lymphatics to adjacent nodes could be visualized after Qdot injection. Parungo *et al.* [54, 55] also applied Qdots to illustrate the lymph drainage patterns of the peritoneum by continued flow to mediastinal lymph nodes. As Qdots can be used to perform multicolor images with high fluorescence intensity, Hama *et al.* [48] used two NIR Qdots with different emission spectra to simultaneously visualize two separate lymphatic flow drainings and variations in the drainage patterns. Kosaka *et al.* [56] used five visually well-distinguishable carboxyl-Qdots (Qdot 545, 565, 585, 605, and 655) injected subdermally into mice at five different sites. *In vivo* lymphatic images successfully distinguished all five lymphatic basins with different colors in real-time (Fig. 1). Kim *et al.* [57] used QDots to visualize SLNs in mouse and pig models. In their study, localization of the SLNs required only 3–4 min, and average detective depth of the SLN in the pig was approximately 1 cm from the skin surface. Knapp *et al.* [58] used NIR Qdots to detect SLNs in invasive urinary bladder cancer in animal models. Near-infrared optical imaging shows promise for imaging superficial lymph drainage. However, poor tissue penetration and photon scattering limited optical imaging to detect deep lymphatic drainage basins [59]. Despite of the limited depth penetration, optical imaging maybe a good complementary technique for intraoperative detection of nodes that have been characterized using more conventional imaging test if dual imaging probes can be developed. For example, magneto-optical probes could allow MRI characterization pre-surgically, and fluorescence-based imaging will lead to confirmation intra-operatively akin to sentinel node imaging. More details about multimodality imaging will be elaborated later.

CT Imaging of Lymph Nodes

As previously mentioned, lymphoscintigraphy and vital blue dye are the two most common methods to map SLNs. One of the major concerns of these methods is their low resolution. CT with appropriate contrast agents, on the other hand, can easily discern enlarged lymph nodes. Wu *et al.* [60] showed in a VX2 carcinoma model that CT-LG was able to identify 96–100% contrast-enhanced SLNs. Suga *et al.* [61] chose a commercially available, water-soluble agent, iopamidol, to visualize breast lymphatic drainage and map breast SLNs in normal dogs and healthy human volunteers. They injected iopamidol into the periareolar skin areas overlying the mammary gland in animals and volunteers, and the connection of SLNs and lymphatic vessels draining from the injection sites can be clearly visualized. Hundred percent SLNs and 87.5% distant nodes resected had a good correlation with the locations and sizes measured by the CT images. In a follow-up study, the same group used CT-LG to evaluate SLNs in patients with operable breast cancer, and the localization of SLNs in all patients could be visualized [62]. Under 3D multidetector-row CT-LG (MDCT-LG) navigation, the sensitivity, false-negative rate, and accuracy of SLN biopsy were 92%, 7%, and 98%, respectively [63]. Margel *et al.* [64, 65] demonstrated that intravenous injection of synthesized iodinated homopolymeric radiopaque nanoparticles allowed enhanced visibility of reticu-

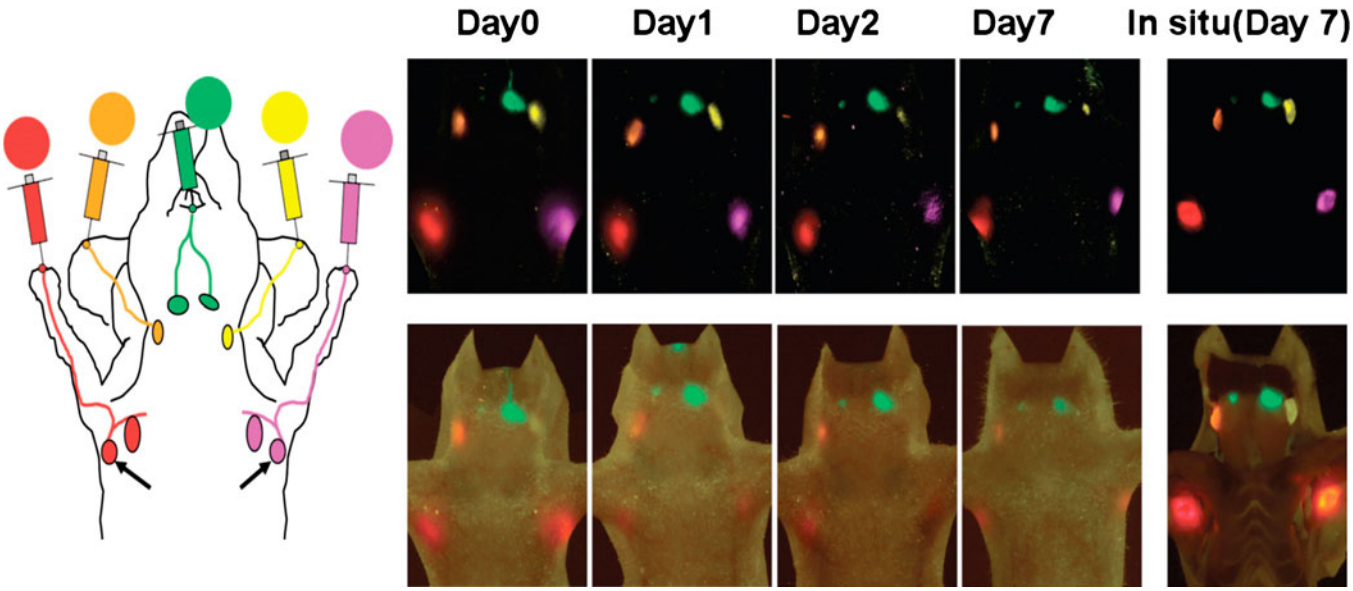

Fig. 1. A five-color optical lymphatic image of lymphatic drainages from the upper extremity (*red*), the ear (*yellow*), and the chin (*green*) obtained using five NIR Qdots (Qdots 655, 585, 545, 565, and 605) from day 1 to day 7. There are less marked reductions in signal, except in the left deep neck lymph node (Qdot 565), and a spectral fluorescence imaging technique is shown together with a schematic illustration (reproduced from Kosaka *et al*. [56] with permission).

loendothelial systems such as lymph nodes, liver, kidneys, and spleen. Rabin *et al*. synthesized a polymer-coated Bi_2S_3 nanoparticle (BPNP) as an injectable CT imaging agent. Following intravenous administration of BPNP, strong vascular enhancement was observed with CT imaging, and the enhancement resulted in clear delineation of the cardiac ventricles and all major arterial and venous structures. In addition, regional lymph nodes were clearly contrasted in mice injected subcutaneously with 50 μl BPNPs [66].

Although the current CT lymphography (CT-LG) is unable to detect occult metastases, it may serve as a viable alternative to lymphoscintigraphy and vital blue dye for SLN identification and guiding SLN biopsies. CT lymphography provides detailed lymphatic anatomy, which may eliminate the potential pitfalls of the lymphoscintigraphy and vital blue dye methods and increase sensitivity and accuracy for SLN biopsy. However, it is difficult for CT to provide information on the flow of lymph owing to the spatial resolution needed and radiation concerns of CT.

MR Imaging of Lymphatic System

Dynamic contrast-enhanced MR imaging (DCE-MRI) is a technique that acquires serial images following the intravenous injection of a contrast agent, and then wash-in and wash-out curves can be derived from designated ROIs for direct comparison. This technique has been widely used to analyze angiogenesis [67, 68]. Ruddell *et al.* [69] developed a DCE-MRI assay to measure changes of lymph flow and lymphatic dysfunction by dynamic mapping of lymphatic drainage in mice models. In their study, B16-F10 melanomas cells were injected into the left hind leg footpad in mice. MR lymphography was scanned with low molecular weight gadolinium contrast agent, Gd-DTPA, which was injected subcutaneously into the dorsal toe of the rear foot to monitor lymph flow dynamically within 3 weeks after implantation. In order to obtain a time course of contrast flow, the kinetics of lymph drainage were examined by taking scans rapidly and repeatedly after Gd-DTPA injection. Results demonstrated that tumor growth in the footpad not only enhanced lymph flow through draining LNs but also enhanced lymph delivery into the heart and vascular circulation. This finding was consistent with the previous hypothesis that tumor-induced lymph flow actively drives metastasis into and through draining LNs [52]. Subcutaneous injection of the conventional extracellular gadolinium-based agents also allows visualization of draining lymph vessels and nodes [70, 71] (Fig. 2). Compared with intravenous injection, the main advantage of interstitial injection is that both lymphatic vessels and lymph nodes can be seen at a lower dose [72]. However, the main problem of these small molecular contrast media is that only small amount can reach the lymphatic system, and others diffuse into the blood system.

Lymphotrophic nanoparticle-enhanced MRI offers a new method for accurate lymph node staging [73]. This technique employs a new class of MR contrast agents with unique biochemical properties including superparamagnetic iron oxide particles (SPIO), liposomes and micelle-forming compounds, and polymers and protein-binding compounds [70, 71, 74]. Ultrasmall superparamagnetic iron oxide (USPIO) contrast may depict salient features of normal and cancer-positive lymph nodes. These nanoparticles are 30 to 50 nm in hydrodynamic size and are composed of an active iron oxide crystalline core and a covering material made of low molecular weight dextran or starch derivatives, which can shorten proton relaxation times, giving a signal distinct from tissue without particles [20, 75]. The small size of the iron oxide nanoparticles enables them to cross capillary walls and localize into lymph nodes either though direct transcapillary passage of the nanoparticles from the venules to the medullary sinuses of lymph nodes or extravasation across permeable capillary beds by a nonselective endothelial transcytosis. Once delivered to the lymph node, the nanoparticles are phagocytosed by macrophages of the reticuloendothelial system (RES), thus causing nanoparticle accumulation within the node [76, 77]. Imaging lymph nodes using USPIO is an indirect way to evaluate macrophage function within the lymph nodes. Accumulation of nanoparticles in benign nodes causes a decrease in signal intensity on T2-weighted and T2*-weighted MRI scans [78]. The RES in malignant lymph nodes lacking normal macrophages cannot phagocytose USPIO and thus retain the bright signals in MRI scans, which was called “negative enhancement” [79]. One disadvantage of USPIO for imaging lymph nodes is the slow transport to the lymphatic system, so post-contrast imaging 24–36 h after contrast media injection is required [80]. In addition, the rather extended pharmacologic half-life of the iron oxide nanoparticles also limited the clinical use [81]. Other disadvantages include the unpredictability of iron-induced susceptibility artifacts, and the heterogeneous enhancement profile in normal lymph nodes [82].

Several limitations of these paramagnetic particles might be overcome with T1-shortening contrast agents. Misselwitz *et al.* [83] detected lymph node metastasis using Gd-carrying liposomes in a guinea pig mode, taking advantage of that, liposomes can be phagocytosed by lymph node macrophages after interstitial injection. Trubetskoy *et al.* [84] also showed that after subcutaneous injection of surface-modified liposomes containing Gd-DTPA phosphatidylethanolamine into the paws of rabbits, axillary and subscapular lymph nodes can be delineated within minutes. Other polymer-based contrast agents have also been tested to image lymph node metastases. Kobayashi *et al.* used different dendrimer-based MRI contrast agents to visualize the anatomy and physiology of deep lymphatic vessels and lymph nodes in mouse models. Among them, PAMAM-G8 was the best for visualizing lymphatic vessels, whereas DAB-G5 was better for visualizing lymph nodes [85–87]. In addition, this group used PAMAM-G6 as a contrast agent and revealed the absence of filling in the metastatic foci of affected lymph nodes. Another dendrimeric agent such as Gadomer-17 was also used for MR imaging of the lymphatic system in

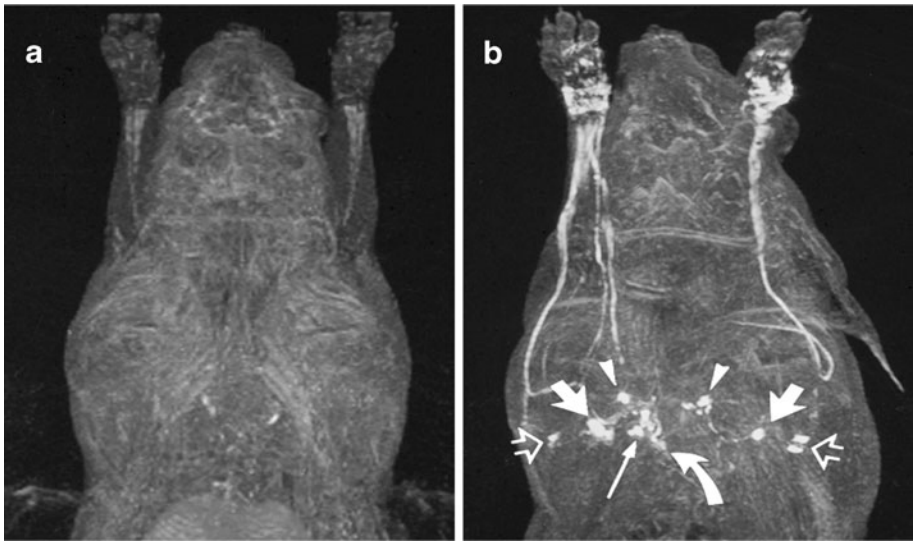

Fig. 2. MRI lymphography demonstrates before (**a**) and 15 min after (**b**) subcutaneous administration of gadoterate meglumine bilaterally in the dorsal aspect of the forepaw. The following lymph node groups are depicted in axillary node, anterior thoracic lymph node (*arrowheads*), parasternal lymph node (*curved arrow*), and mediastinal lymph node (*long solid arrow*; reproduced from Ruehm *et al*. [70] with permission).

different experimental models [88, 89]. Herborn *et al*. [74] used a new blood-pool contrast agent, MS-325, to image regional lymph nodes. MS-325 is albumin-binding Gd-based contrast agent, which protein-binding properties may make this agent large enough to be phagocytosed and lymphotropically cleared. After interstitial injection, lymphatic vessels and tumor-bearing lymph nodes can be detected clearly.

It is of note that the route of administration can be an issue for clinical translation. Interstitial and subcutaneous injections are viable techniques to study lymphatic pathways but are not suited to image and stage nodes which are better served with intravenous agent injection and delivery. This is important when staging needs characterization of nodes in regional distribution.

Ultrasound Imaging of Lymphatic System

Since the first description of contrast-enhanced ultrasound imaging (CEUS) by Gramiak and Shah [90], it has been widely used in both preclinical experiments and clinical diagnosis. In general, there are several advantages of CEUS such as low cost, high spatial resolution (comparable to MRI or CT and greater than PET or SPECT), and high contrast sensitivity and signal-to-noise ratio (comparable to PET and SPECT). These advantages make CEUS a promising imaging modality for detecting SLNs.

Microbubbles are the most widely used ultrasound contrast agents. The microbubble shell can be made with lipids, denatured albumin, or polymers incorporating polyethylene glycol in order to reduce gas diffusion into the blood, to reduce recognition by the immune system, and to enhance stability [91, 92]. Based on the specific acoustic properties, microbubbles can be sensitively imaged with regular ultrasound methods. For CEUS imaging of SLNs, microbubbles were injected directly into tissues of interest. In animal studies, ultrasound contrast agents have been shown to accumulate in SLNs but not second-order lymph nodes. The mechanisms of this passive targeting are poorly understood but probably related to the avidity of the shell material for macrophages [93]. Lurie *et al.* [94] injected perfluoropropane-filled microbubble contrast medium into peritumoral tissues in ten dogs with spontaneous head or neck tumors and compared the results with lymphoscintigraphy in which dogs were injected peritumorally with ^{99m}Tc-sulfur colloid. CEUS could identify SLNs and associated lymphatics, and the results were consistent with lymphoscintigraphy findings, indicating that CEUS might be an effective adjunct or alternative to conventional techniques for SLN detection and localization.

Nielsen *et al.* investigated whether the distance from the contrast agent injection site to SLN could affect the detectability of CEUS in a swine model. The result showed that the distance did not interfere with SLN detection [95]. In a pilot clinical trial, before surgery, patients with breast cancer received a periareolar intradermal injection of microbubbles; lymphatic channels were visualized immediately by ultrasonography and followed to identify putative axillary SLNs. The sensitivity of SLN detection in this study was 89% [96].

Besides SLN detection, microbubbles have also been used to differentiate benign and malignant lymph nodes. The mechanism is probably that microbubbles are phagocytosed by macrophages or reticuloendothelial cells and appear bright on an ultrasonogram in benign lymph nodes, and malignant lymph nodes that lack reticuloendothelial cells cannot take up the microbubbles and would remain

hypoechoic. Goldberg *et al.* demonstrated that the accuracy of SLN detection by CEUS and lymphoscintigraphy was 90% and 81%, respectively, in a swine model with melanoma. Compared with histological examination, the sensitivity, specificity, and accuracy for correctly depicting metastases in swine SLNs by lymphatic CEUS were 95%, 63%, and 86%, respectively [97].

The main disadvantages of US are its poor spatial resolution, the large size of the microbubble and hence its slower rate of uptake, its limited use in the thorax and deep retroperitoneum, and its dependence on operator experience [98]. Indeed, microbubble-CEUS of the lymph nodes is unlikely to reflect either the extravasation of bubbles, with re-uptake by the lymphatic system, or uptake by macrophages and tracking to lymph nodes, due to the size of the contrast agents and the timing of scanning, respectively [1].

Photoacoustic Imaging of Lymphatic System

Photoacoustic imaging (PAI), as a hybrid biomedical imaging modality, is developed based on the photoacoustic effect. In PAI, non-ionizing laser pulses are delivered into biological tissues. Some of the delivered energy will be absorbed and converted into heat, leading to transient thermoelastic expansion and thus ultrasonic emission. The generated ultrasonic waves are then detected by ultrasonic transducers to form images. The advantage of PAI is that it retains high optical contrast while overcoming the poor spatial resolution of pure optical imaging and provides good spatial resolution by detecting ultrasound, which has relatively low scattering [99, 100].

PAI in combination with different contrast agents is promising in improved detection of metastases. Song *et al.* [101] tried methylene blue as a PAI contrast agent to image SLNs in rats and were able to detect lesions about 2–3 cm in depth. Other groups also used a series of nanoparticle-based contrast agents such as carbon nanotubes, gold nanocages, gold nanorods, and gold nanobeacons to improve resolution and allow deep tissue imaging [102–104]. The single-walled carbon nanotubes (SWNTs) were first applied as a PA contrast agent by the Stanford group for imaging tumor integrin expression [102]. Later on, Pramanik *et al.* [105] used carbon nanotube-enhanced photoacoustic identification of SLNs in a rat model. Recently, Pan *et al.* [104] demonstrated near-infrared detection of SLN with gold nanobeacons (GNBs) providing the photoacoustic contrast in a rodent model. They found that smaller GNBs were noted trafficking through the lymphatic system and accumulating more efficiently in the lymph nodes in comparison to the bigger nanoagents. Within 1 h post-injection, the contrast ratio of the lymph nodes with the surrounding blood vessels was 9:1 [104] (Fig. 3).

McCormack *et al.* [106] used photoacoustic method to detect SLN micrometastasis in a melanoma model nodes. In their study, HS 936 human melanoma cells were separated and injected into the canine lymph nodes. Because melanoma cells contain melanin, which can absorb the light and produce photoacoustic pulses under laser, these photoacoustic pulses can be detected by special sensors. Photoacoustic responses from a lymph node with as few as 500 melanoma cells can be detected, while normal lymph nodes showed no response. In addition, recent study on photoacoustic detection and photothermal ablation of individual light-absorbing nanoparticles labeled tumor cells in lymph nodes *in vivo* will encourage further explorations of light-absorbing nanoparticles in biomedical applications, in particular noninvasive and target-specific lymphatic diagnosis and therapy [103].

PET Imaging of Lymphatic System

So far, PET is the most sensitive and specific technique for imaging molecular pathways *in vivo* in humans [107]. PET radiotracers are physiologically and pharmacologically relevant compounds labeled with positron-emitting radioisotopes (such as fluoride-18 or carbon-11). After internalization by injection or inhalation, the tracer reaches the target, and the location and the quantity are then detected with a PET scanner. The inherent sensitivity and specificity of PET is the major strength of this technique. Isotopes can be detected down to the 100-pM level in the target tissues. At this low level, the compounds often have little or no physiological effect on the patient or the test animal, which permits studying the mechanism of action or biodistribution independent of any physiological consequences [108, 109]. The spatial resolution of PET down to the millimeter level permits applications not only to humans for diagnosis and drug development but also to animals for preclinical studies. The ability of PET to translate studies from animals to humans adds to its appeal. 2-deoxy-2-[^{18}F]fluoro-D-glucose (^{18}F-FDG) is now the most commonly used PET tracer worldwide. ^{18}F-FDG PET has been used to image metastases and detect metastatic spread of malignant cells to regional lymph nodes in a wide variety of tumor types [110]. ^{18}F-FDG PET is able to detect increased glycolytic rate in cancer cells compared to normal cells; therefore, PET can functionally assess lymph nodes and potentially detect metastases in normal-sized nodes. When PET is combined with a CT scan (PET–CT), the fused image can demonstrate increased metabolism with its anatomical location. Besides FDG, other molecules specifically metabolized in tumor cells have also been tested to evaluate LN status. Choline is a molecule that is metabolized into phosphorylcholine and is incorporated into cellular membranes [111]. It can be labeled with ^{18}F and ^{11}C. ^{11}C-choline sensitivity and specificity for LN metastasis in prostate cancer have been studied, which could detect metastasis with a sensitivity of 80%, a specificity of 96%, and an accuracy of 93% [112]. However, one limitation with the use of ^{11}C-choline as a tracer is its short half-life. In a recent clinical study recruiting 132 patients with prostate cancer, the sensitivity, specificity, and

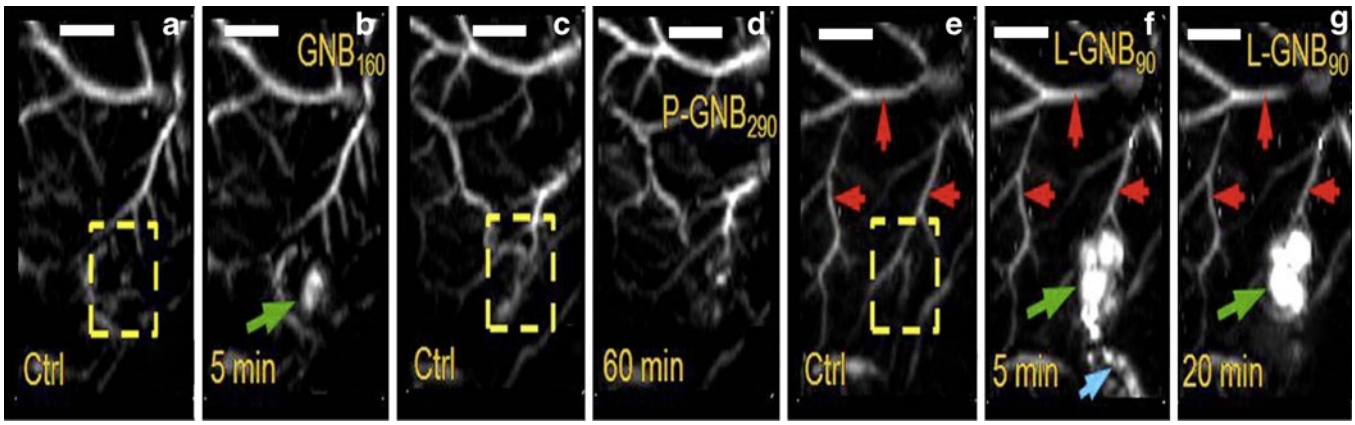

Fig. 3. *In vivo* noninvasive photoacoustic imaging of sentinel lymph nodes in rat. Lymph node is not visible in a 60-min post-injection image of nanobeacons P-GNB$_{160}$, (**d**) but SLNs are clearly visible after L-GNB$_{90}$ injection (10 nm; **g**; reproduced from Pan *et al*. [104] with permission).

positive and negative predictive values of ^{18}F-fluorocholine PET/CT in the detection of malignant LNs were 45%, 96%, 82%, and 83%, respectively. For LN metastases greater than or equal to 5 mm in diameter, sensitivity, specificity, and positive and negative predictive values were 66%, 96%, 82%, and 92%, respectively [113]. ^{11}C-acetate or ^{18}F-acetate reflects another aspect of lipid metabolism. Fricke *et al.* [114] demonstrated that ^{11}C-acetate is better than ^{18}F-FDG in detecting local recurrences and regional lymph node metastases of prostate cancer. In addition to the above-mentioned PET tracers, other positron-emitting molecules such as anti-1-amino-3-^{18}F-fluorocyclobutane-1-carboxylic acid (anti-^{18}F-FACBC), 16β-^{18}F-fluoro-5α-dihydrotestosterone (^{18}F-FDHT), and ^{11}C-methionine have also been used to detect LN metastasis [115]. However, the anatomical resolution of PET (approximately 4–8 mm^3 in clinical and 1–2 mm^3 in small animal imaging systems) is noticeably poorer than that achieved by CT or MRI [116]. Due to the relatively lower resolution of PET as compared to other anatomical imaging techniques, PET allows for detecting malignancy in normal-sized nodes but is insufficient for detecting small nodes, thus preventing its application in staging tumors like breast, rectum, *etc*. Indeed, in breast cancer patients, the sensitivity, specificity, PPV, NPV, and accuracy of FDG PET/CT was 58%, 92%, 82%, 77%, and 79%, indicating that FDG PET/CT cannot replace invasive approaches for axillary staging but may extend the indication for SLNB [117]. Low sensitivity of PET/CT also has been reported in patients with primary malignant melanoma [118].

Multi-modal Imaging

Among the above-mentioned imaging techniques, no single modality is perfect and sufficient to gain all the necessary information [119, 120]. Therefore, the combination of multiple imaging techniques can offer synergistic advantages [121]. Multi-modal imaging can be achieved either through the combination of imaging hardware such as PET/CT and SPECT/CT [122], through the combination of different contrast agents [123], or through co-registration of images acquired with different modalities. With regard to lymphatic imaging, this leads to improved accuracy and sensitivity of lymph nodes detection as well as lymphatic drainage visualization.

The combination of PET and CT has been matured into an important clinical diagnostic tool. The underlying principle of PET/CT systems is the acquisition of two dedicated imaging procedures, CT and PET, in a single step followed by image co-registration, which are able to provide anatomical and functional data sets in a single session with accurate image co-registration [124]. In this way, The CT component of the hybrid system is used to improve anatomical definition of the ROIs for analysis and to create radiation-attenuation maps to correct for non-uniform attenuation [125]. Clinical studies have demonstrated the advantages of PET/CT over separately performed PET and CT, particularly in the field of oncology [126]. A number of clinical studies compared FDG–PET/CT with CT alone for evaluating lymph nodes for metastatic spread. The results demonstrated that sensitivity, specificity, positive predictive value, negative predictive value, and accuracy of lymph node staging were all significantly improved with FDG–PET/CT [127, 128]. SPECT/CT is based on the similar principles of PET/CT. Hybrid SPECT/CT lymphoscintigraphic imaging facilitates the localization of SLNs by showing the relationships between SLNs and important anatomic structures, which enables precise SLN localization and helps to ensure minimal dissection in clinical application [129].

With the development of microPET or microPET/CT scanners dedicated to small animal imaging studies, it can provide a similar *in vivo* imaging capability in mice, rats, monkeys, and humans so one can readily transfer knowledge and molecular measurements between species [130, 131].

Along with the progress made in several key techniques including identifying scintillators with adequate magnetic properties, in developing suitable PET detectors which use optical fibers to guide the scintillation light away from the MR magnetic fields or that replace the PMTs by magnetic field-insensitive avalanche photodiodes (APD) [132], several research groups have successfully developed small PET/MRI prototypes for small-animal studies [133, 134] and even a human-sized prototype design for neurology applications [135]. With the PET/MRI system, three functional imaging techniques will be united including PET, fMRI, and spectroscopy with morphological MRI, offering far more potential than just tracing biomarkers and displaying anatomy [134].

Most of the contrast agents for lymphatic imaging generally have one function and can only be imaged in monochrome. When radiocolloid and dye are used in tandem, there is a lower false-negative rate for sentinel node localization when compared with using either agent alone [136, 137]. Combination of both radioactive and color signals into a single dose has also been investigated such as ^{99m}Tc-dextran-dyes [27], ^{99m}Tc-/^{111}In-phthalocyanine tetrasulfonate [138], ^{125}I-methylene blue [139], and ^{99m}Tc-EB [140]. Tsopelas *et al.* [140] confirmed that both the soluble ^{99m}Tc-EB and ^{99m}Tc-antimony trisulfide colloid (ATC) discriminated the SLNs up to 50 min after administration. However, ^{99m}Tc-EB had the advantage of providing radioactive (gamma probe) and color signals simultaneously during the operative exposure.

Kobayashi et al. [121] synthesized ^{111}In-labeled radionuclide/five-color NIR optical dualmodal imaging probes using a polyamidoamine dendrimer (generation-6 PAMAM dendrimer) with an ethylenediamine core as the platform component. Radionuclide imaging of this dual modal imaging probe allows increased depth penetration and absolute quantification, whereas multicolor NIR optical imaging offers excellent real-time spatial resolution and the ability to distinguish multiple lymphatic drainages. Both of these methods have a matched high sensitivity that allows for a minimization of the required injection dose [121]. Koyama et al. [141] synthesized MR/NIR optical hybrid contrast agent GdG6-Cy5.5 to perform anatomic MRL and NIR imaging with one injection. A number of nanoparticle-based PET/MRI dual modality or optical/PET/MIR triple modality probes [142–144] showed promising results in tumor imaging. These probes may also have the potential to be applied for multimodality imaging of the lymphatic system. By combining strong optical contrast and high ultrasonic resolution in a single modality, photoacoustic tomography of lymph node demonstrated the potential to be used clinically for accurate, noninvasive imaging of SLNs for axillary lymph node staging [145]. With a modified clinical US imaging system, photoacoustic images of rat SLNs clearly help visualize methylene blue accumulation, whereas coregistered photoacoustic/US images depict lymph node positions relative to surrounding anatomy [146].

Active Targeting Biomarkers-Based Imaging of Lymphatics

Tumor blood vessels express molecular markers that distinguish them from normal blood vessels [147]. Recent data indicate that lymphatic endothelial cells are structurally different from blood endothelial cells and also express lymphatic system specific marker molecules such as podoplainin, Prox-1, LYVE-1, and VEGFR-3 [148–150]. Recent technical developments in optical imaging and other imaging modalities, in conjunction with these molecular markers, help to better understand the mechanisms underlying lymphangiogenesis and lymphatic metastases of tumor.

McElroy *et al.* [151] used AlexaFluor-labeled anti-mouse lymphatic endothelial hyaluronan receptor-1 (LYVE-1) monoclonal antibody to image mouse lymphatics and real-time track the movement of tumor cells engineered to express red-fluorescent protein (RFP) within the green fluorescently labeled lymphatic vessels in a mouse model. In their study, they created a ventral skin flap to expose the inguinal, axillary lymph nodes, and the interconnecting lymphatics of the anterior abdominal wall, and then injected AlexaFluor-labeled monoclonal anti-mouse LYVE-1 into the tissues around the exposed inguinal lymph node. The draining inguinal lymphatics and the afferent lymphatics of the receiving axillary lymph nodes were clearly shown after antibody delivery. After *in vivo* staining of mouse lymphatic endothelium, human pancreatic tumor cells expressing RFP were injected into the inguinal lymph node and surrounding tissues. Tumor cell trafficked along green labeled lymphatics could be reliably seen (Fig. 4). This study apparently improved the understanding on interactions of primary tumors with lymphatic system and lymphatic dissemination of cancer cells.

Using *in vivo* phage display technology, Laakkonen *et al.* [150, 152] identified a panel of peptides that home to lymphatic blood endothelial cells. Among them, a 9-amino-acid cyclic peptide (CGNKRTRGC) named as LyP-1 indeed had tumor homing specificity. In their study, intravenous injection of FITC-LyP-1 led to prominent accumulation in the tumor tissue 16–20 h after intravenous injection [153]. The extraordinary homing efficiency and ability to recognize metastatic lesions suggest the potential diagnostic uses for LyP-1.

The active targeting strategies can also be applied with ultrasound after attaching antibodies, peptides, or other molecules to microbubble shell [92]. Examples include lipid shell microbubbles attached anti-ICAM-1 monoclonal antibody for imaging acute cardiac allograft transplant rejection in rats, microbubbles targeted to vascular endothelial growth factor receptor type 2 (VEGFR2) for imaging tumor angiogenesis in two murine tumor models, and microbubbles bear a covalently bound RGD peptide for targeting thrombosis

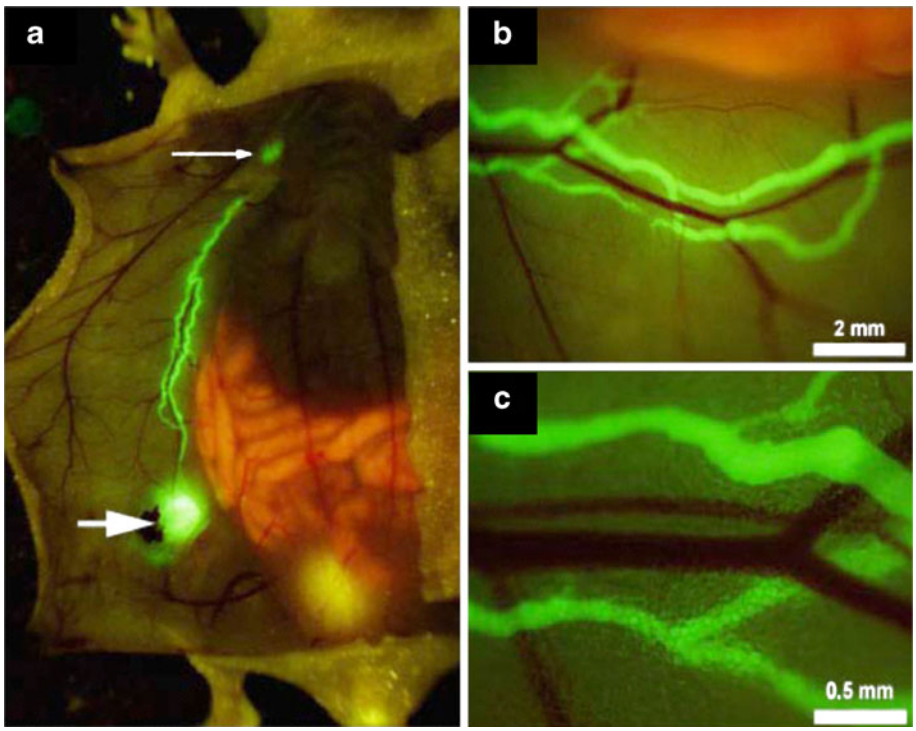

Fig. 4. Fluorescence imaging of *in vivo* of the inguinal lymph nodes (*larger arrow*), axillary (*small arrow*), and the connecting lymphatics of the anterior abdominal wall after delivery of AlexaFluor-conjugated monoclonal anti-mouse LYVE-1 antibody (**a**–**c**). Neighboring blood vessels did not stain (**b**, **c**; reproduced from McElroy *et al*. [151] with permission).

and angiogenesis [154–157]. Li *et al.* [158] synthesized LyP-1 ultrasonic microbubbles and demonstrated the potential of this bubble conjugate for imaging tumor lymphatic vessels and as a targeted drug delivery vehicle to treat lymph node metastasis. Hauff *et al.* [159] used L-selectin ligand-specific air-filled microparticles to target peripheral lymph nodes in normal mice and dogs. In their study, an L-selectin ligand, MECA-79 antigen, was selected for lymph node targeting. After intravenous administration of MECA-79 antibody conjugated polymer shell microbubbles, all the cervical, inguinal, axillary, popliteal, and mesenteric lymph nodes in mice and the popliteal lymph nodes in dogs showed stimulated acoustic emission (SAE) signals.

Currently, ongoing PET studies are attempting to better detect micrometastases in lymph nodes using molecular reporter genes. One of these promising reporters is the

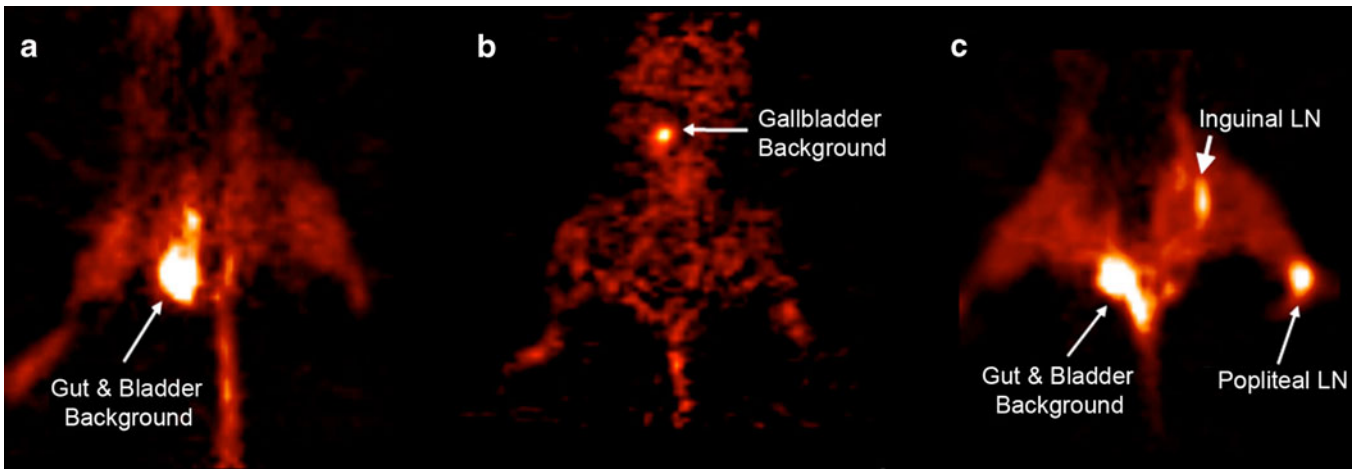

Fig. 5. [^{18}F] FEAU-PET imaging of mice. **a** A control tumor-bearing mice with saline injection, and (**b**) mice without tumor injected with NV1023 had [^{18}F] FEAU signal levels similar to background. **c** Positive PET signal was detected in mice with positive popliteal and inguinal lymph node metastases injected with NV1023 (reproduced from Brader *et al*. [162] with permission).

modified form of the herpes simplex type 1 thymidine kinase gene (HSV1-tk): HSV1-sr39tk. The protein sr39tk is a mutated form of the HSV-tk gene that can phosphorylate more than ten different substrates including ^{18}F-FHBG and ^{18}F-FEAU [160]. When these positron-emitting molecules are phosphorylated by sr39tk protein, the product is trapped in the cells and can be detected by PET–CT through its ^{18}F positron-emitting isotope [161]. Brader *et al.* [162] demonstrated the feasibility of using recombinant human herpes simplex virus (HSV) vectors to detect nodal metastases in a human melanoma model by intratumoral injections of HSV NV1023 and intravenous injection of [^{18}F]FEAU (Fig. 5). In addition to functioning as a PET reporter gene, the gene encoding the sr39tk reporter also acts as a suicide gene. Coupling detection and suicide gene therapy would enable not only the accurate assessment of lymph node status but also the prospect of preventing metastatic outgrowth and systemic spread. Gambhir group has developed a two-step transcriptional amplification (TSTA) system [163] to increase the accuracy of imaging and the precise location of nodes. Based on this strategy, they developed several prostate-specific adenoviral vectors that express imaging reporter genes under the control of a highly amplified prostate-specific antigen (PSA) promoter system (TSTA) [164]. Burton *et al.* injected PSA–TSTA adenovirus in conjunction with its tracer ^{18}F-FHBG into mouse forepaws in a LAPC9 prostate tumor xenograft model. Once in the node, the PSA–TSTA adenovirus can infect prostate tumor cells present there and activate the prostate restricted expression of an imaging reporter gene. This genetic biomarker-based PET was able to decisively seek out lymph node metastasis in a mouse bearing 2.5-mm lymph node lesions [164].

Summary

The lymphatic vessel system imaging is an emerging field of research. It has long been overshadowed by research on angiogenesis because of the lack of imaging modalities to visualize and quantitatively assess lymphatic vasculature *in vitro* and *in vivo*. These difficulties were overcome partially during the past few years based on the discovery of lymphatic specific molecular markers and improvement of resolution and sensitivity of imaging modalities. Especially these new imaging modalities contributed to the rapid expansion of our knowledge on the mechanisms underlying lymphatic development and the diseases associated with lymphatic dysfunction. However, efforts are still needed, especially on several critical aspects including (1) optimization of multimodality probes to take full synergistic advantage of each single imaging modality and minimize drawback; (2) combination of imaging probes and therapeutic agents to realize theranostic effect for lymphatic targeted therapies; (3) identification of novel lymphangiogenic markers and development of imaging probes with high affinity and specificity; and (4) development of imaging strategies to improve the ability of visualizing micrometastases within lymph nodes.

Acknowledgments. F. Zhang and G. Lu are supported by the National Natural Science Foundation of China (NSFC grant No. 30930028) and 973 grants (2006, CB705707, China). G. Niu is an Imaging Sciences Training Program (ISTP) Fellow jointly supported by the Radiology and Imaging Sciences Department, NIH Clinical Center and the Intramural Research Program, NIBIB, NIH. This research was supported by the Intramural Research Program of the NIBIB, NIH. We acknowledge Dr. Henry S. Eden for critically reading this manuscript.

Conflict of interest. The authors declare that they have no conflict of interest.

References

1. Barrett T, Choyke PL, Kobayashi H (2006) Imaging of the lymphatic system: new horizons. Contrast Media Mol Imaging 1:230–245
2. Zawieja D (2005) Lymphatic biology and the microcirculation: past, present and future. Microcirculation 12:141–150
3. Mumprecht V, Detmar M (2009) Lymphangiogenesis and cancer metastasis. J Cell Mol Med 13:1405–1416
4. Alitalo K, Tammela T, Petrova TV (2005) Lymphangiogenesis in development and human disease. Nature 438:946–953
5. Mandriota SJ, Jussila L, Jeltsch M et al (2001) Vascular endothelial growth factor-C-mediated lymphangiogenesis promotes tumour metastasis. EMBO J 20:672–682
6. Skobe M, Hawighorst T, Jackson DG et al (2001) Induction of tumor lymphangiogenesis by VEGF-C promotes breast cancer metastasis. Nat Med 7:192–198
7. Swartz MA, Skobe M (2001) Lymphatic function, lymphangiogenesis, and cancer metastasis. Microsc Res Tech 55:92–99
8. Hirakawa S, Brown LF, Kodama S et al (2007) VEGF-C-induced lymphangiogenesis in sentinel lymph nodes promotes tumor metastasis to distant sites. Blood 109:1010–1017
9. Bruyere F, Noel A (2010) Lymphangiogenesis: *in vitro* and *in vivo* models. FASEB J 24:8–21
10. He Y, Rajantie I, Pajusola K et al (2005) Vascular endothelial cell growth factor receptor 3-mediated activation of lymphatic endothelium is crucial for tumor cell entry and spread via lymphatic vessels. Cancer Res 65:4739–4746
11. Tammela T, Alitalo K (2010) Lymphangiogenesis: molecular mechanisms and future promise. Cell 140:460–476
12. Nakamura K, Rockson SG (2007) Biomarkers of lymphatic function and disease: state of the art and future directions. Mol Diagn Ther 11:227–238
13. Rinderknecht M, Detmar M (2008) Tumor lymphangiogenesis and melanoma metastasis. J Cell Physiol 216:347–354
14. Pepper MS, Tille JC, Nisato R, Skobe M (2003) Lymphangiogenesis and tumor metastasis. Cell Tissue Res 314:167–177
15. Ristimaki A, Narko K, Enholm B, Joukov V, Alitalo K (1998) Proinflammatory cytokines regulate expression of the lymphatic endothelial mitogen vascular endothelial growth factor-C. J Biol Chem 273:8413–8418
16. Saban MR, Memet S, Jackson DG et al (2004) Visualization of lymphatic vessels through NF-kappaB activity. Blood 104:3228–3230
17. Wilting J, Becker J, Buttler K, Weich HA (2009) Lymphatics and inflammation. Curr Med Chem 16:4581–4592
18. Moriguchi P, Sannomiya P, Lara PF et al (2005) Lymphatic system changes in diabetes mellitus: role of insulin and hyperglycemia. Diabetes Metab Res Rev 21:150–157
19. Harvey NL, Srinivasan RS, Dillard ME et al (2005) Lymphatic vascular defects promoted by Prox1 haploinsufficiency cause adult-onset obesity. Nat Genet 37:1072–1081
20. Sharma R, Wendt JA, Rasmussen JC et al (2008) New horizons for imaging lymphatic function. Ann NY Acad Sci 1131:13–36
21. Moghimi SM, Rajabi-Siahboomi R (1996) Advanced colloid-based systems for efficient delivery of drugs and diagnostic agents to the lymphatic tissues. Prog Biophys Mol Biol 65:221–249
22. Petrova TV, Karpanen T, Norrmen C et al (2004) Defective valves and abnormal mural cell recruitment underlie lymphatic vascular failure in lymphedema distichiasis. Nat Med 10:974–981

23. Rodrigues EB, Costa EF, Penha FM et al (2009) The use of vital dyes in ocular surgery. Surv Ophthalmol 54:576–617
24. Heath TJ, Brandon RA, Norman ST (1984) Drainage of lymph from the foreleg to the superficial cervical lymph node in sheep. Res Vet Sci 37:66–71
25. Kajiya K, Hirakawa S, Detmar M (2006) Vascular endothelial growth factor-A mediates ultraviolet B-induced impairment of lymphatic vessel function. Am J Pathol 169:1496–1503
26. Modi S, Stanton AW, Mortimer PS, Levick JR (2007) Clinical assessment of human lymph flow using removal rate constants of interstitial macromolecules: a critical review of lymphoscintigraphy. Lymphat Res Biol 5:183–202
27. Pereira CT, Luiz Navarro Marques F, Williams J, Wlademir De Martin B, Primo Bombonato P (2008) 99mTc-labeled dextran for mammary lymphoscintigraphy in dogs. Vet Radiol Ultrasound 49:487–491
28. Anthony JP, Foster RD, Price DC, Mahdavian M, Inoue Y (1997) Lymphatic regeneration following microvascular limb replantation: a qualitative and quantitative animal study. J Reconstr Microsurg 13:327–330
29. Alex JC, Krag DN (1993) Gamma-probe guided localization of lymph nodes. Surg Oncol 2:137–143
30. Czerniecki BJ, Bedrosian I, Faries M, Alavi A (2001) Revolutionary impact of lymphoscintigraphy and intraoperative sentinel node mapping in the clinical practice of oncology. Semin Nucl Med 31:158–164
31. Nakashima K, Kurebayashi J, Sonoo H et al (2010) Preoperative dynamic lymphoscintigraphy predicts sentinel lymph node metastasis in patients with early breast cancer. Breast Cancer 17:17–21
32. Harivardhan RL, Sharma RK, Chuttani K, Mishra AK, Murthy RS (2005) Influence of administration route on tumor uptake and biodistribution of etoposide loaded solid lipid nanoparticles in Dalton's lymphoma tumor bearing mice. J Control Release 105:185–198
33. Boinpally RR, Zhou SL, Devraj G et al (2004) Iontophoresis of lecithin vesicles of cyclosporin A. Int J Pharm 274:185–190
34. Holm R, Porter CJ, Edwards GA et al (2003) Examination of oral absorption and lymphatic transport of halofantrine in a triple-cannulated canine model after administration in self-microemulsifying drug delivery systems (SMEDDS) containing structured triglycerides. Eur J Pharm Sci 20:91–97
35. Kim J, Chung KH, Lee CM et al (2008) Lymphatic delivery of 99mTc-labeled dextran acetate particles including cyclosporine A. J Microbiol Biotechnol 18:1599–1605
36. Mehnert W, Mader K (2001) Solid lipid nanoparticles: production, characterization and applications. Adv Drug Deliv Rev 47:165–196
37. Videira MA, Botelho MF, Santos AC et al (2002) Lymphatic uptake of pulmonary delivered radiolabelled solid lipid nanoparticles. J Drug Target 10:607–613
38. Lucarelli RT, Ogawa M, Kosaka N et al (2009) New approaches to lymphatic imaging. Lymphat Res Biol 7:205–214
39. Delaey E, van Laar F, De Vos D et al (2000) A comparative study of the photosensitizing characteristics of some cyanine dyes. J Photochem Photobiol B 55:27–36
40. Landsman ML, Kwant G, Mook GA, Zijlstra WG (1976) Light-absorbing properties, stability, and spectral stabilization of indocyanine green. J Appl Physiol 40:575–583
41. Branch RA, James JA, Read AE (1976) The clearance of antipyrine and indocyanine green in normal subjects and in patients with chronic lever disease. Clin Pharmacol Ther 20:81–89
42. Kwon S, Sevick-Muraca EM (2007) Noninvasive quantitative imaging of lymph function in mice. Lymphat Res Biol 5:219–231
43. Sharma R, Wang W, Rasmussen JC et al (2007) Quantitative imaging of lymph function. Am J Physiol Heart Circ Physiol 292:H3109–H3118
44. Hirche C, Murawa D, Mohr Z, Kneif S, Hunerbein M (2010) ICG fluorescence-guided sentinel node biopsy for axillary nodal staging in breast cancer. Breast Cancer Res Treat 121:373–378
45. Murawa D, Hirche C, Dresel S, Hunerbein M (2009) Sentinel lymph node biopsy in breast cancer guided by indocyanine green fluorescence. Br J Surg 96:1289–1294
46. Fujiwara M, Mizukami T, Suzuki A, Fukamizu H (2009) Sentinel lymph node detection in skin cancer patients using real-time fluorescence navigation with indocyanine green: preliminary experience. J Plast Reconstr Aesthet Surg 62:e373–e378
47. Ghoroghchian PP, Therien MJ, Hammer DA (2009) *In vivo* fluorescence imaging: a personal perspective. Wiley Interdiscip Rev Nanomed Nanobiotechnol 1:156–167
48. Hama Y, Koyama Y, Urano Y, Choyke PL, Kobayashi H (2007) Two-color lymphatic mapping using Ig-conjugated near infrared optical probes. J Invest Dermatol 127:2351–2356
49. Dubertret B, Skourides P, Norris DJ et al (2002) *In vivo* imaging of quantum dots encapsulated in phospholipid micelles. Science 298:1759–1762
50. Gao X, Cui Y, Levenson RM, Chung LW, Nie S (2004) *In vivo* cancer targeting and imaging with semiconductor quantum dots. Nat Biotechnol 22:969–976
51. Michalet X, Pinaud FF, Bentolila LA et al (2005) Quantum dots for live cells, *in vivo* imaging, and diagnostics. Science 307:538–544
52. Harrell MI, Iritani BM, Ruddell A (2007) Tumor-induced sentinel lymph node lymphangiogenesis and increased lymph flow precede melanoma metastasis. Am J Pathol 170:774–786
53. Ballou B, Ernst LA, Andreko S et al (2007) Sentinel lymph node imaging using quantum dots in mouse tumor models. Bioconjug Chem 18:389–396
54. Parungo CP, Colson YL, Kim SW et al (2005) Sentinel lymph node mapping of the pleural space. Chest 127:1799–1804
55. Parungo CP, Soybel DI, Colson YL et al (2007) Lymphatic drainage of the peritoneal space: a pattern dependent on bowel lymphatics. Ann Surg Oncol 14:286–298
56. Kosaka N, Ogawa M, Sato N, Choyke PL, Kobayashi H (2009) *In vivo* real-time, multicolor, quantum dot lymphatic imaging. J Invest Dermatol 129:2818–2822
57. Kim S, Lim YT, Soltesz EG et al (2004) Near-infrared fluorescent type II quantum dots for sentinel lymph node mapping. Nat Biotechnol 22:93–97
58. Knapp DW, Adams LG, Degrand AM et al (2007) Sentinel lymph node mapping of invasive urinary bladder cancer in animal models using invisible light. Eur Urol 52:1700–1708
59. Harrell MI, Iritani BM, Ruddell A (2008) Lymph node mapping in the mouse. J Immunol Methods 332:170–174
60. Wu H, Xu X, Ying H et al (2009) Preliminary study of indirect CT lymphography-guided sentinel lymph node biopsy in a tongue VX2 carcinoma model. Int J Oral Maxillofac Surg 38:1268–1272
61. Suga K, Ogasawara N, Okada M, Matsunaga N (2003) Interstitial CT lymphography-guided localization of breast sentinel lymph node: preliminary results. Surgery 133:170–179
62. Suga K, Yuan Y, Okada M et al (2004) Breast sentinel lymph node mapping at CT lymphography with iopamidol: preliminary experience. Radiology 230:543–552
63. Suga K, Yamamoto S, Tangoku A et al (2005) Breast sentinel lymph node navigation with three-dimensional interstitial multidetector-row computed tomographic lymphography. Invest Radiol 40:336–342
64. Aviv H, Bartling S, Kieslling F, Margel S (2009) Radiopaque iodinated copolymeric nanoparticles for X-ray imaging applications. Biomaterials 30:5610–5616
65. Galperin A, Margel D, Baniel J et al (2007) Radiopaque iodinated polymeric nanoparticles for X-ray imaging applications. Biomaterials 28:4461–4468
66. Rabin O, Manuel PJ, Grimm J, Wojtkiewicz G, Weissleder R (2006) An X-ray computed tomography imaging agent based on long-circulating bismuth sulphide nanoparticles. Nat Mater 5:118–122
67. Sun MR, Ngo L, Genega EM et al (2009) Renal cell carcinoma: dynamic contrast-enhanced MR imaging for differentiation of tumor subtypes–correlation with pathologic findings. Radiology 250:793–802
68. Kobayashi H, Shirakawa K, Kawamoto S et al (2002) Rapid accumulation and internalization of radiolabeled herceptin in an inflammatory breast cancer xenograft with vasculogenic mimicry predicted by the contrast-enhanced dynamic MRI with the macromolecular contrast agent G6-(1B4M-Gd)(256). Cancer Res 62:860–866
69. Ruddell A, Harrell MI, Minoshima S et al (2008) Dynamic contrast-enhanced magnetic resonance imaging of tumor-induced lymph flow. Neoplasia 10:706–713, 701 p following 713
70. Ruehm SG, Corot C, Debatin JF (2001) Interstitial MR lymphography with a conventional extracellular gadolinium-based agent: assessment in rabbits. Radiology 218:664–669
71. Ruehm SG, Schroeder T, Debatin JF (2001) Interstitial MR lymphography with gadoterate meglumine: initial experience in humans. Radiology 220:816–821
72. Misselwitz B (2006) MR contrast agents in lymph node imaging. Eur J Radiol 58:375–382
73. Kobayashi H, Kawamoto S, Brechbiel MW et al (2005) Detection of lymph node involvement in hematologic malignancies using micro-

magnetic resonance lymphangiography with a gadolinum-labeled dendrimer nanoparticle. Neoplasia 7:984–991
74. Herborn CU, Lauenstein TC, Vogt FM et al (2002) Interstitial MR lymphography with MS-325: characterization of normal and tumor-invaded lymph nodes in a rabbit model. AJR Am J Roentgenol 179:1567–1572
75. Mouli SK, Zhao LC, Omary RA, Thaxton CS (2010) Lymphotropic nanoparticle enhanced MRI for the staging of genitourinary tumors. Nat Rev Urol 7:84–93
76. Feldman AS, McDougal WS, Harisinghani MG (2008) The potential of nanoparticle-enhanced imaging. Urol Oncol 26:65–73
77. Saokar A, Braschi M, Harisinghani MG (2006) Lymphotrophic nanoparticle enhanced MR imaging (LNMRI) for lymph node imaging. Abdom Imaging 31:660–667
78. Weissleder R, Elizondo G, Wittenberg J et al (1990) Ultrasmall superparamagnetic iron oxide: an intravenous contrast agent for assessing lymph nodes with MR imaging. Radiology 175:494–498
79. Bellin MF, Beigelman C, Precetti-Morel S (2000) Iron oxide-enhanced MR lymphography: initial experience. Eur J Radiol 34:257–264
80. Harisinghani MG, Dixon WT, Saksena MA et al (2004) MR lymphangiography: imaging strategies to optimize the imaging of lymph nodes with ferumoxtran-10. Radiographics 24:867–878
81. Weissleder R, Stark DD, Engelstad BL et al (1989) Superparamagnetic iron oxide: pharmacokinetics and toxicity. AJR Am J Roentgenol 152:167–173
82. Taupitz M, Wagner S, Hamm B, Binder A, Pfefferer D (1993) Interstitial MR lymphography with iron oxide particles: results in tumor-free and VX2 tumor-bearing rabbits. AJR Am J Roentgenol 161:193–200
83. Misselwitz B, Sachse A (1997) Interstitial MR lymphography using Gd-carrying liposomes. Acta Radiol Suppl 412:51–55
84. Trubetskoy VS, Cannillo JA, Milshtein A, Wolf GL, Torchilin VP (1995) Controlled delivery of Gd-containing liposomes to lymph nodes: surface modification may enhance MRI contrast properties. Magn Reson Imaging 13:31–37
85. Kobayashi H, Kawamoto S, Choyke PL et al (2003) Comparison of dendrimer-based macromolecular contrast agents for dynamic micro-magnetic resonance lymphangiography. Magn Reson Med 50:758–766
86. Kobayashi H, Kawamoto S, Star RA et al (2003) Micro-magnetic resonance lymphangiography in mice using a novel dendrimer-based magnetic resonance imaging contrast agent. Cancer Res 63:271–276
87. Kobayashi H, Kawamoto S, Sakai Y et al (2004) Lymphatic drainage imaging of breast cancer in mice by micro-magnetic resonance lymphangiography using a nano-size paramagnetic contrast agent. J Natl Cancer Inst 96:703–708
88. Staatz G, Spuntrup E, Klosterhalfen B et al (2005) High-resolution T1-weighted MR-lymphography of inguinal lymph nodes after interstitial application of Gadomer-17 in animal experiments. Rofo 177:968–974
89. Torchia MG, Misselwitz B (2002) Combined MR lymphangiography and MR imaging-guided needle localization of sentinel lymph nodes using Gadomer-17. AJR Am J Roentgenol 179:1561–1565
90. Gramiak R, Shah PM, Kramer DH (1969) Ultrasound cardiography: contrast studies in anatomy and function. Radiology 92:939–948
91. Voigt JU (2009) Ultrasound molecular imaging. Methods 48:92–97
92. Dayton PA, Rychak JJ (2007) Molecular ultrasound imaging using microbubble contrast agents. Front Biosci 12:5124–5142
93. Lindner JR, Coggins MP, Kaul S et al (2000) Microbubble persistence in the microcirculation during ischemia/reperfusion and inflammation is caused by integrin- and complement-mediated adherence to activated leukocytes. Circulation 101:668–675
94. Lurie DM, Seguin B, Schneider PD, Verstraete FJ, Wisner ER (2006) Contrast-assisted ultrasound for sentinel lymph node detection in spontaneously arising canine head and neck tumors. Invest Radiol 41:415–421
95. Nielsen KR, Grossjohann HS, Hansen CP, Nielsen MB (2008) Use of contrast-enhanced ultrasound imaging to detect the first draining lymph node (FDLN) in a swine model: correlation of imaging findings with the distance from the injection site to the FDLN. J Ultrasound Med 27:1203–1209
96. Sever A, Jones S, Cox K et al (2009) Preoperative localization of sentinel lymph nodes using intradermal microbubbles and contrast-enhanced ultrasonography in patients with breast cancer. Br J Surg 96:1295–1299
97. Goldberg BB, Merton DA, Liu JB et al (2004) Sentinel lymph nodes in a swine model with melanoma: contrast-enhanced lymphatic US. Radiology 230:727–734
98. Ravizzini G, Turkbey B, Barrett T, Kobayashi H, Choyke PL (2009) Nanoparticles in sentinel lymph node mapping. Wiley Interdiscip Rev Nanomed Nanobiotechnol 1:610–623
99. Song KH, Stoica G, Wang LV (2006) *In vivo* three-dimensional photoacoustic tomography of a whole mouse head. Opt Lett 31:2453–2455
100. Wang X, Pang Y, Ku G et al (2003) Noninvasive laser-induced photoacoustic tomography for structural and functional *in vivo* imaging of the brain. Nat Biotechnol 21:803–806
101. Song KH, Stein EW, Margenthaler JA, Wang LV (2008) Noninvasive photoacoustic identification of sentinel lymph nodes containing methylene blue *in vivo* in a rat model. J Biomed Opt 13:054033
102. De la Zerda A, Zavaleta C, Keren S et al (2008) Carbon nanotubes as photoacoustic molecular imaging agents in living mice. Nat Nanotechnol 3:557–562
103. Kim JW, Galanzha EI, Shashkov EV, Moon HM, Zharov VP (2009) Golden carbon nanotubes as multimodal photoacoustic and photothermal high-contrast molecular agents. Nat Nanotechnol 4:688–694
104. Pan D, Pramanik M, Senpan A et al (2010) Near infrared photoacoustic detection of sentinel lymph nodes with gold nanobeacons. Biomaterials 31:4088–4093
105. Pramanik M, Song KH, Swierczewska M et al (2009) *In vivo* carbon nanotube-enhanced non-invasive photoacoustic mapping of the sentinel lymph node. Phys Med Biol 54:3291–3301
106. McCormack D, Al-Shaer M, Goldschmidt BS et al (2009) Photoacoustic detection of melanoma micrometastasis in sentinel lymph nodes. J Biomech Eng 131:074519
107. Jones T (1996) The imaging science of positron emission tomography. Eur J Nucl Med 23:807–813
108. Phelps ME, Hoffman EJ, Mullani NA, Ter-Pogossian MM (1975) Application of annihilation coincidence detection to transaxial reconstruction tomography. J Nucl Med 16:210–224
109. Phelps ME (2000) PET: the merging of biology and imaging into molecular imaging. J Nucl Med 41:661–681
110. Schoder H, Glass EC, Pecking AP et al (2006) Molecular targeting of the lymphovascular system for imaging and therapy. Cancer Metastasis Rev 25:185–201
111. Machtens S, Serth J, Meyer A et al (2007) Positron emission tomography (PET) in the urooncological evaluation of the small pelvis. World J Urol 25:341–349
112. de Jong IJ, Pruim J, Elsinga PH, Vaalburg W, Mensink HJ (2003) Preoperative staging of pelvic lymph nodes in prostate cancer by 11C-choline PET. J Nucl Med 44:331–335
113. Beheshti M, Imamovic L, Broinger G et al (2010) 18F choline PET/CT in the preoperative staging of prostate cancer in patients with intermediate or high risk of extracapsular disease: a prospective study of 130 patients. Radiology 254:925–933
114. Fricke E, Machtens S, Hofmann M et al (2003) Positron emission tomography with 11C-acetate and 18F-FDG in prostate cancer patients. Eur J Nucl Med Mol Imaging 30:607–611
115. Larson SM, Schoder H (2009) New PET tracers for evaluation of solid tumor response to therapy. Q J Nucl Med Mol Imaging 53:158–166
116. Willmann JK, van Bruggen N, Dinkelborg LM, Gambhir SS (2008) Molecular imaging in drug development. Nat Rev Drug Discov 7:591–607
117. Heusner TA, Kuemmel S, Hahn S et al (2009) Diagnostic value of full-dose FDG PET/CT for axillary lymph node staging in breast cancer patients. Eur J Nucl Med Mol Imaging 36:1543–1550
118. Klode J, Dissemond J, Grabbe S et al (2010) Sentinel lymph node excision and PET-CT in the initial stage of malignant melanoma: a retrospective analysis of 61 patients with malignant melanoma in American Joint Committee on Cancer stages I and II. Dermatol Surg 36:439–445
119. Niu G, Cai W, Chen X (2008) Molecular imaging of human epidermal growth factor receptor 2 (HER-2) expression. Front Biosci 13:790–805
120. Cai W, Niu G, Chen X (2008) Multimodality imaging of the HER-kinase axis in cancer. Eur J Nucl Med Mol Imaging 35:186–208
121. Kobayashi H, Koyama Y, Barrett T et al (2007) Multimodal nanoprobes for radionuclide and five-color near-infrared optical lymphatic imaging. ACS Nano 1:258–264
122. Cai W, Chen X (2008) Multimodality molecular imaging of tumor angiogenesis. J Nucl Med 49(Suppl 2):113S–128S

123. Lee S, Chen X (2009) Dual-modality probes for *in vivo* molecular imaging. Mol Imaging 8:87–100
124. Veit P, Ruehm S, Kuehl H et al (2006) Lymph node staging with dual-modality PET/CT: enhancing the diagnostic accuracy in oncology. Eur J Radiol 58:383–389
125. Kamel E, Hany TF, Burger C et al (2002) CT vs 68Ge attenuation correction in a combined PET/CT system: evaluation of the effect of lowering the CT tube current. Eur J Nucl Med Mol Imaging 29:346–350
126. Townsend DW (2008) Dual-modality imaging: combining anatomy and function. J Nucl Med 49:938–955
127. Antoch G, Stattaus J, Nemat AT et al (2003) Non-small cell lung cancer: dual-modality PET/CT in preoperative staging. Radiology 229:526–533
128. Lardinois D, Weder W, Hany TF et al (2003) Staging of non-small-cell lung cancer with integrated positron-emission tomography and computed tomography. N Engl J Med 348:2500–2507
129. Mar MV, Miller SA, Kim EE, Macapinlac HA (2007) Evaluation and localization of lymphatic drainage and sentinel lymph nodes in patients with head and neck melanomas by hybrid SPECT/CT lymphoscintigraphic imaging. J Nucl Med Technol 35:10–16, quiz 17-20
130. Cherry SR, Shao Y, Silverman RW et al (1997) MicroPET: a high resolution PET scanner for imaging small animals. IEEE Trans Nucl Sci 44:1161–1166
131. Chatziioannou AF, Cherry SR, Shao Y et al (1999) Performance evaluation of microPET: a high-resolution lutetium oxyorthosilicate PET scanner for animal imaging. J Nucl Med 40:1164–1175
132. Delso G, Ziegler S (2009) PET/MRI system design. Eur J Nucl Med Mol Imaging 36(Suppl 1):S86–S92
133. Catana C, Procissi D, Wu Y et al (2008) Simultaneous *in vivo* positron emission tomography and magnetic resonance imaging. Proc Natl Acad Sci USA 105:3705–3710
134. Judenhofer MS, Wehrl HF, Newport DF et al (2008) Simultaneous PET-MRI: a new approach for functional and morphological imaging. Nat Med 14:459–465
135. Schlemmer HP, Pichler BJ, Schmand M et al (2008) Simultaneous MR/PET imaging of the human brain: feasibility study. Radiology 248:1028–1035
136. Kim T, Giuliano AE, Lyman GH (2006) Lymphatic mapping and sentinel lymph node biopsy in early-stage breast carcinoma: a metaanalysis. Cancer 106:4–16
137. Wong SL, Edwards MJ, Chao C et al (2001) Sentinel lymph node biopsy for breast cancer: impact of the number of sentinel nodes removed on the false-negative rate. J Am Coll Surg 192:684–689, discussion 689-691
138. El-Tamer M, Saouaf R, Wang T, Fawwaz R (2003) A new agent, blue and radioactive, for sentinel node detection. Ann Surg Oncol 10:323–329
139. Stafford SJ, Wright JL, Schwimer J et al (2006) Development of 125I-methylene blue for sentinel lymph node biopsy. J Surg Oncol 94:293–297
140. Tsopelas C, Bellon M, Bevington E et al (2008) Lymphatic mapping with 99mTc-Evans Blue dye in sheep. Ann Nucl Med 22:777–785
141. Koyama Y, Talanov VS, Bernardo M et al (2007) A dendrimer-based nanosized contrast agent dual-labeled for magnetic resonance and optical fluorescence imaging to localize the sentinel lymph node in mice. J Magn Reson Imaging 25:866–871
142. Chen K, Xie J, Xu H et al (2009) Triblock copolymer coated iron oxide nanoparticle conjugate for tumor integrin targeting. Biomaterials 30:6912–6919
143. Lee HY, Li Z, Chen K et al (2008) PET/MRI dual-modality tumor imaging using arginine-glycine-aspartic (RGD)-conjugated radiolabeled iron oxide nanoparticles. J Nucl Med 49:1371–1379
144. Xie J, Chen K, Huang J et al (2010) PET/NIRF/MRI triple functional iron oxide nanoparticles. Biomaterials 31:3016–3022
145. Wang LV (2008) Prospects of photoacoustic tomography. Med Phys 35:5758–5767
146. Erpelding TN, Kim C, Pramanik M et al (2010) Sentinel lymph nodes in the rat: noninvasive photoacoustic and US imaging with a clinical US system. Radiology 256:102–110
147. Niu G, Chen X (2009) PET imaging of angiogenesis. PET Clin 4:17–38
148. Banerji S, Ni J, Wang SX et al (1999) LYVE-1, a new homologue of the CD44 glycoprotein, is a lymph-specific receptor for hyaluronan. J Cell Biol 144:789–801
149. Breiteneder-Geleff S, Soleiman A, Horvat R et al (1999) Podoplanin–a specific marker for lymphatic endothelium expressed in angiosarcoma. Verh Dtsch Ges Pathol 83:270–275
150. Laakkonen P, Porkka K, Hoffman JA, Ruoslahti E (2002) A tumor-homing peptide with a targeting specificity related to lymphatic vessels. Nat Med 8:751–755
151. McElroy M, Hayashi K, Garmy-Susini B et al (2009) Fluorescent LYVE-1 antibody to image dynamically lymphatic trafficking of cancer cells *in vivo*. J Surg Res 151:68–73
152. Laakkonen P, Zhang L, Ruoslahti E (2008) Peptide targeting of tumor lymph vessels. Ann NY Acad Sci 1131:37–43
153. Laakkonen P, Akerman ME, Biliran H et al (2004) Antitumor activity of a homing peptide that targets tumor lymphatics and tumor cells. Proc Natl Acad Sci USA 101:9381–9386
154. Weller GE, Lu E, Csikari MM et al (2003) Ultrasound imaging of acute cardiac transplant rejection with microbubbles targeted to intercellular adhesion molecule-1. Circulation 108:218–224
155. Korpanty G, Carbon JG, Grayburn PA, Fleming JB, Brekken RA (2007) Monitoring response to anticancer therapy by targeting microbubbles to tumor vasculature. Clin Cancer Res 13:323–330
156. Wright WH Jr, McCreery TP, Krupinski EA et al (1998) Evaluation of new thrombus-specific ultrasound contrast agent. Acad Radiol 5(Suppl 1):S240–S242
157. Willmann JK, Paulmurugan R, Chen K et al (2008) US imaging of tumor angiogenesis with microbubbles targeted to vascular endothelial growth factor receptor type 2 in mice. Radiology 246:508–518
158. Li X, Jin Q, Chen T et al (2009) LyP-1 ultrasonic microbubbles targeting to cancer cell as tumor bio-acoustics markers or drug carriers: targeting efficiency evaluation in, microfluidic channels. Conf Proc IEEE Eng Med Biol Soc 2009:463–466
159. Hauff P, Reinhardt M, Briel A, Debus N, Schirner M (2004) Molecular targeting of lymph nodes with L-selectin ligand-specific US contrast agent: a feasibility study in mice and dogs. Radiology 231:667–673
160. Yaghoubi SS, Gambhir SS (2006) PET imaging of herpes simplex virus type 1 thymidine kinase (HSV1-tk) or mutant HSV1-sr39tk reporter gene expression in mice and humans using [18F]FHBG. Nat Protoc 1:3069–3075
161. Pouliot F, Johnson M, Wu L (2009) Non-invasive molecular imaging of prostate cancer lymph node metastasis. Trends Mol Med 15:254–262
162. Brader P, Kelly K, Gang S et al (2009) Imaging of lymph node micrometastases using an oncolytic herpes virus and [F]FEAU PET. PLoS ONE 4:e4789
163. Iyer M, Wu L, Carey M et al (2001) Two-step transcriptional amplification as a method for imaging reporter gene expression using weak promoters. Proc Natl Acad Sci USA 98:14595–14600
164. Burton JB, Johnson M, Sato M et al (2008) Adenovirus-mediated gene expression imaging to directly detect sentinel lymph node metastasis of prostate cancer. Nat Med 14:882–888